

## Chimeras Unfolded

Georgi S. Medvedev<sup>1</sup> • Matthew S. Mizuhara<sup>2</sup>

Received: 24 May 2021 / Accepted: 15 January 2022 © The Author(s), under exclusive licence to Springer Science+Business Media, LLC, part of Springer Nature 2022

#### **Abstract**

The instability of mixing in the Kuramoto model of coupled phase oscillators is the key to understanding a range of spatiotemporal patterns, which feature prominently in collective dynamics of systems ranging from neuronal networks, to coupled lasers, to power grids. In this paper, we describe a codimension-2 bifurcation of mixing whose unfolding, in addition to the classical scenario of the onset of synchronization, also explains the formation of clusters and chimeras. We use a combination of linear stability analysis and Penrose diagrams to identify and analyze a variety of spatiotemporal patterns including stationary and traveling coherent clusters and twisted states, as well as their combinations with regions of incoherent behavior called chimera states. Penrose diagrams are used to locate the bifurcation of mixing and to determine its type. The linear stability analysis, on the other hand, yields the velocity distribution of the pattern emerging from the bifurcation. Furthermore, we show that network topology can endow chimera states with nontrivial spatial organization. In particular, we present twisted chimera states, whose coherent regions are organized as stationary or traveling twisted states. The analytical results are illustrated with numerical bifurcation diagrams computed for the Kuramoto model with uni-, bi-, and trimodal frequency distributions and all-to-all and nonlocal nearest-neighbor connectivity.

#### 1 Introduction

The Kuramoto model (KM) on a graph sequence  $(\Gamma^n)$  describes collective dynamics in coupled networks. It is given by the following system of ordinary differential equations

$$\dot{\theta}_i = \omega_i + 2Kn^{-1} \sum_{j=1}^n a_{ij}^n \sin(\theta_j - \theta_i + \alpha), \quad i \in [n] := \{1, 2, \dots, n\}.$$
 (1.1)

Communicated by Shin-ichi Sasa.

☑ Georgi S. Medvedev medvedev@drexel.edu

Matthew S. Mizuhara mizuharm@tcnj.edu

Published online: 08 February 2022

- <sup>1</sup> Department of Mathematics, Drexel University, Philadelphia, PA, USA
- Department of Mathematics and Statistics, The College of New Jersey, Ewing Township, NJ, USA



Here,  $\theta_i: \mathbb{R}^+ \to \mathbb{T} := \mathbb{R}/2\pi\mathbb{Z}$ , stands for the phase of oscillator i;  $\omega_i$ 's are independent random intrinsic frequencies drawn from a distribution with density  $g(\omega)$ , and K is the strength of coupling.  $(a_{ij}^n)$  is the  $n \times n$  symmetric (weighted) adjacency matrix of  $\Gamma^n$ , a graph on n nodes, which defines the connectivity of the network. The phase lag  $\alpha$  controls the type of coupling and can play a role in pattern formation [1, 28]. It will not be used in the main part of this work and, thus,  $\alpha$  is set to 0 until Sect. 5.

**Remark 1.1** The factor 2 in front of the coupling term in the formulation of the model (1.1) saves from using 2's in multiple formulae throughout the paper. This factor is not used in the classical formulation of the KM [18].

Despite its analytical simplicity, the KM provides important insights into general principles underlying network dynamics. It is best known for revealing a universal scenario of transition to synchronization, identified in a variety of systems from neuronal networks, to coupled lasers, to power grids [36, 39]. More recently, the KM became the main framework for studying chimera states, counterintuitive patterns combining regions of coherent and incoherent dynamics [1, 19, 20, 27, 28, 30, 34]. For a long time, coherence and incoherence were viewed as distinct regimes in network dynamics. Computational and experimental studies of chimeras clearly demonstrate that coexistence of coherence and incoherence is ubiquitous in diverse physical and biochemical systems [13, 26, 28, 34, 37]. Since the discovery of chimera states by Kuramoto and Battogtokh in 2002 [19], there has been a continuous stream of papers suggesting different dynamical mechanisms for their generation. Many such studies rely heavily on numerical simulations. The most complete analytical information about chimera states was derived using the Ott-Antonsen Ansatz [2, 20, 23, 27, 28, 33], which exploits the symmetries of the KM. When applicable, the Ott-Antonsen Ansatz provides a powerful tool for studying chimera states. However, not all chimera states lie in the Ott-Antonsen manifold (see [28] for a discussion of the benefits and limitations of the Ott-Antonsen Ansatz).

In the present paper, we describe a bifurcation scenario which connects mixing to clusters to chimeras. At the heart of this scenario lies a codimension-two bifurcation of mixing, whose unfolding contains clusters and chimeras. We use the linear stability analysis of mixing [6] and Penrose diagrams [11, 35] to locate different bifurcations and to describe statistical properties of the patterns emerging from them. We relate pitchfork (PF) and Andronov-Hopf (AH) bifurcations to the appearance of synchronized stationary and traveling clusters. The eigenfunctions of the linearized operator corresponding to bifurcating eigenvalues capture the velocity distributions within partially locked states (PLS) and chimera states emerging when mixing loses stability. Furthermore, Penrose diagrams provide a crisp picture of the bifurcation scenarios in the KM and suggest the domain of existence of chimera states. A rigorous center manifold reduction at bifurcations of mixing in the KM is a very technical problem [3, 5, 7, 11]. As was pointed out in [10], a good deal of information about spatiotemporal patterns emerging at the loss of stability of mixing can be learned from the linear stability analysis. In the present paper, we develop this idea further paying closer attention to the bifurcation scenarios connecting mixing to chimera states in the KM with multimodal frequency distributions.

After a brief review of the linear stability analysis of mixing following [6, 9] in Sect.2, we turn to the analysis of bifurcations in the KM with uni-, bi- and tri- modal frequency distribution in Sect. 3. We start with the unimodal distribution to explain how to use Penrose diagrams to locate the bifurcations in the KM (cf. [11]) and how to use linearization to determine patterns born at this bifurcation. Then we apply this method to study bifurcations



Chimeras Unfolded Page 3 of 19 46

in the KM with bimodal frequency distributions. Here, we identify the codimension-2 PF-AH bifurcation which is responsible for the emergence of clusters in the KM model. By breaking symmetry of the bimodal frequency distribution, we locate chimeras and clusters bifurcating from mixing. To illustrate bifurcations in the KM with multimodal distributions more fully we also discuss bifurcations in the KM with trimodal frequency distributions. Here, as in the bimodal case, we identify a master bifurcation of mixing, whose unfolding contains bifurcation scenarios connecting mixing to chimeras and three-cluster states. In Sect. 4, we address the effects of the network connectivity on spatial organization of patterns emerging from the bifurcations of mixing. To this end, we show that nonlocal nearest-neighbor connectivity transforms the clusters of synchronized behavior into clusters of twisted states. In particular, we demonstrate various patterns involving stationary and traveling twisted states, as well as twisted chimera states. We conclude with a brief discussion of the results of this work in Sect. 5.

# 2 Stability of Mixing

A starting point in virtually any approach to the analysis of chimera states is the thermodynamic limit as the size of the system n tends to  $\infty$ . Clearly, to expect a common limiting behavior of solutions of the discrete problems (1.1), the corresponding graphs ( $\Gamma^n$ ) need to have a well defined asymptotic behavior as  $n \to \infty$  as well. To this end, we assume that ( $\Gamma^n$ ) is a convergent sequence of dense graphs, whose limit is given by a symmetric measurable function  $W: [0, 1]^2 \to [0, 1]$ . Functions representing graphs and graph limits are called graphons [22]. Many common types of network connectivity, including random connectivity, used in the models of coupled dynamical systems can be defined by simple graphons (cf. [6, 15]).

In this paper, we consider connectivity of two types: all-to-all and nonlocal nearest-neighbor. To describe the former we need  $W(x, y) \equiv 1$ . The latter is assigned by W(x, y) = V(x - y), where

$$V(x) = \mathbf{1}_{(-r,r)}(x)$$
 on  $(-1/2, 1/2)$  (2.1)

and is extended to  $\mathbb{R}$  by periodicity. Here,  $\mathbf{1}_A$  stands for the indicator function of A and  $r \in (0, 1/2)$  a fixed parameter describing the range of connectivity. Then the nearest–neighbor connectivity in (1.1) is assigned by setting  $a_{ij}^n = 1$  when  $\left[\frac{i-1}{n}, \frac{i}{n}\right) \times \left[\frac{j-1}{n}, \frac{j}{n}\right)$ ,  $i, j \in [n]$ , has a nonempty intersection with the support of W, and  $a_{ij}^n = 0$  otherwise.

For the KM on a convergent family of graphs defined by W, the thermodynamic limit has the following form [15]

$$\partial_t f(t, \theta, \omega, x) + \partial_\theta \{ V(t, \theta, \omega, x) f(t, \theta, \omega, x) \} = 0, \tag{2.2}$$

where  $f(t, \theta, \omega, x)d\theta d\omega$  is the probability that the state of the oscillator at point  $x \in I := [0, 1]$  at time  $t \in \mathbb{R}^+$  is in  $(\theta, \theta + d\theta) \times (\omega, \omega + d\omega)$ . The unit interval I represents a continuum of oscillators in the limit  $n \to \infty$ . The velocity field is derived from the right-hand side of (1.1):

$$V(t,\theta,\omega,x) = \omega - Ki\left(\kappa(t,x)e^{-i\theta} - \overline{\kappa(t,x)e^{-i\theta}}\right),\tag{2.3}$$



where

$$\kappa(t,x) = \int_{\mathbb{T}} e^{i\theta} \int_{\mathbb{R}} \left( \mathbf{W} f(t,\theta,\omega,\cdot) \right) (x) d\omega d\theta, \tag{2.4}$$

$$(\mathbf{W}\phi)(x) = \int_{I} W(x, y)\phi(y)dy. \tag{2.5}$$

The function  $\kappa(t,x)$  is called a local order parameter. Here, we use a modified order parameter adapted to the analysis of the KM on graphs [6] (see [18] for the original definition). The order parameter  $\kappa(t,x)$  provides a convenient measure of coherence in network dynamics at  $x \in I$  at time t. The self-adjoint operator W is determined by W, which in turn reflects the asymptotic connectivity of the network. A rigorous justification of the mean field limit (2.2) in the context of the KM with all-to-all coupling was given in [21]. For the KM on convergent graph sequences, the use of the Vlasov equation as a mean field limit was further justified in [6, 17].

Equation (2.2) has a steady state solution

$$f_{mix} = \frac{g(\omega)}{2\pi},\tag{2.6}$$

which is called mixing. It corresponds to the uniform distribution of the phases over  $\mathbb{T}$ . Stability of mixing for the KM on graphs was analyzed in [6]. For completeness, we outline the main steps of the linear stability analysis below.

It is convenient to study stability of  $f_{mix}$  in the Fourier space. To this end, we introduce

$$u_l(t,\omega,x) = \int_{\mathbb{T}} e^{il\theta} f(t,\theta,\omega,x) d\theta, \quad l \in \mathbb{Z}.$$
 (2.7)

Note that

$$u_0(t, \omega, x) = \int_{\mathbb{T}} f(t, \theta, \omega, x) d\theta = g(\omega). \tag{2.8}$$

By applying the Fourier transform to (2.2) and keeping only the linear terms, we have

$$\partial_t u_1(t,\omega,\cdot) = i\,\omega u_1(t,\omega,\cdot) + Kg(\omega)W\left[\int_{\mathbb{R}} u_1(t,\omega,\cdot)d\omega\right],\tag{2.9}$$

$$\partial_t u_l(t, \omega, \cdot) = i l \omega u_l(t, \omega, \cdot), \quad l \ge 1.$$
 (2.10)

It was sufficient to restrict to  $l \ge 1$  in (2.10) because f is real and thus  $u_{-l} = \bar{u}_l$ .

Further, the steady state  $f_{mix}$  is mapped to  $u_{mix} = (g(\omega), 0, 0, ...)$  in the Fourier space. Equations in (2.10) describe pure transport. Thus, the stability of  $u_{mix}$  is decided by (2.9), which we rewrite as

$$\partial_t v = T[v], \tag{2.11}$$

where

$$T[\upsilon](\omega,\cdot) = i\,\omega\upsilon + Kg(\omega)W\left[\int_{\mathbb{R}} \upsilon(\xi,\cdot)d\xi\right], \quad \upsilon \in \mathcal{H} = L^2\left(\mathbb{R} \times [0,1]\right). \tag{2.12}$$

As an operator on  $\mathcal{H}$ , T has continuous spectrum on  $i\mathbb{R}$  (cf. [6]). To locate the eigenvalues of T, we consider the following spectral problem

$$T[\upsilon] = \lambda \upsilon, \quad \upsilon \in \mathcal{H}.$$
 (2.13)

Using (2.12), we rewrite (2.13) as follows

$$K\frac{g(\omega)}{\lambda - i\omega} \mathbf{W} \left[ \int_{\mathbb{R}} \upsilon(\xi, \cdot) d\xi \right] = \upsilon(\omega, \cdot). \tag{2.14}$$

Chimeras Unfolded Page 5 of 19 46

By integrating both parts of (2.14) over  $\mathbb{R}$ , we arrive at

$$KG(\lambda)W[w] = w, (2.15)$$

where  $w = \int_{\mathbb{R}} v(\xi, \cdot) d\xi \in L^2([0, 1])$  and

$$G(\lambda) = \int_{\mathbb{R}} \frac{g(\omega)d\omega}{\lambda - i\,\omega}.\tag{2.16}$$

As a compact self-adjoint operator on  $L^2([0, 1])$ , W has a countable sequence of real eigenvalues with a single accumulation point at 0 [14]. Let  $\mu$  be an arbitrary fixed nonzero eigenvalue of W and let  $w_{\mu}$  be a corresponding eigenfunction. From (2.15), we find the following equation for the eigenvalues of T:

$$G(\lambda) = \frac{1}{K\mu}.\tag{2.17}$$

A root of (2.17) is an eigenvalue of T. The corresponding eigenfunction is then found from (2.14)

$$v_{\lambda}(\omega, x) = \Upsilon_{\lambda}(\omega) w_{\mu}(x), \quad \Upsilon_{\lambda}(\omega) = \frac{g(\omega)}{\lambda - i\omega}.$$
 (2.18)

For  $\lambda \notin i\mathbb{R}$ ,  $\Upsilon_{\lambda}$  is a holomorphic function. Since we are interested in bifurcations of mixing, we need to resolve the meaning of  $\Upsilon_{\lambda}$  for  $\lambda \in i\mathbb{R}$ . To this end, we impose the following assumptions on the class of admissible probability density functions  $g \in L^1([0, 1])$ . Following [11], we assume that the Fourier transform of  $g, \hat{g} \in C(\mathbb{R})$  and

$$\sup_{t \in \mathbb{R}} e^{at} \left| \hat{g}(t) \right| < \infty \tag{2.19}$$

for some a > 0. Under these assumptions,  $\Upsilon_{iy}$  can be viewed as a tempered distribution [9]. Specifically, for any  $\phi$  from the Schwartz class  $\mathcal{S}(\mathbb{R})$ , by the Sokhotski–Plemelj formula (cf. [38]), we have

$$\begin{split} \langle \Upsilon_{iy}, \phi \rangle &= \lim_{\lambda \to i \, y + 0} \int_{-\infty}^{\infty} \frac{g(\omega)\phi(\omega)}{\lambda + i \, y - i \, \omega} d\omega \\ &= \lim_{\lambda \to 0 +} \int_{-\infty}^{\infty} \frac{g(\omega + y)\phi(\omega + y)}{\lambda - i \, \omega} d\omega \\ &= \pi \, g(y)\phi(y) - i \, \text{pv} \int_{-\infty}^{\infty} \frac{g(\omega + y)\phi(\omega + y)}{\omega} d\omega. \end{split}$$

Thus,  $\Upsilon_{iy} \in \mathcal{S}'(\mathbb{R})$  and

$$\Upsilon_{iy} = \pi g(y)\delta_y - i\mathcal{P}_y[g], \qquad (2.20)$$

where  $\delta_{y}$  stands for the Dirac delta function centered at y and

$$\langle \mathcal{P}_{y}[g], \phi \rangle = \text{pv} \int_{-\infty}^{\infty} \frac{g(\omega + y)\phi(\omega + y)}{\omega} d\omega.$$

In particular,

$$\Upsilon_0 = \pi g(0)\delta_0 - i\mathcal{P}_0[g],\tag{2.21}$$

The eigenfunctions (2.18), (2.20) corresponding to bifurcating eigenvalues will be used to explain spatiotemporal patterns arising at the loss of stability of mixing.



46 Page 6 of 19 G. S. Medvedev, M. S. Mizuhara

# 3 Bifurcations: From Mixing to Chimeras

In this section, we describe a sequence of bifurcations from mixing to clusters to chimeras. We will show that all these structures belong to the unfolding of a codimension-2 bifurcation of mixing, the central object of our study. For the KM forced by small noise, this bifurcation was studied by Crawford [16]. In the following section, we will discuss the role of W in shaping chimera states. Until then, we restrict to  $W \equiv 1$ . This corresponds to all-to-all connectivity. The bifurcation scenarios discussed below will also hold for the KM on any graph sequence with a constant graph limit, e.g., Erdős-Rényi or Paley graphs [8]. For  $W \equiv 1$ , the only nonzero eigenvalue of W is  $\mu = 1$ . Thus, the equation for the eigenvalues of T (2.17) takes the following form

$$G(z) = K^{-1}, (3.1)$$

where G is defined in (2.16).

A rigorous analysis of bifurcations in this model requires generalized spectral theory [4]. This is related to the fact that as an operator on  $L^2(\mathbb{R} \times [0,1])$ , T has a continuous spectrum filling the imaginary axis. Thus, to be able to trace the eigenvalues crossing the imaginary axis under the variation of K, T has to be given a more general interpretation. For the KM on graphs this was done in [6] extending the analysis of the classical KM in [4]. In the present paper, to avoid the technicalities of generalized spectral theory, we take the following approach. We locate the eigenvalues of T in  $\mathbb{H}^+ = \{z \in \mathbb{C} : \operatorname{Re} z > 0\}$ , where the corresponding eigenfunctions are still in  $L^2(\mathbb{R} \times [0,1])$ . Then we trace these eigenvalues until they hit the imaginary axis and identify the corresponding bifurcations. As soon as the spectral parameter  $\lambda$  hits the imaginary axis, the corresponding eigenfunctions leave  $L^2(\mathbb{R} \times [0,1])$ . From this point, they are interpreted as tempered distributions (cf. (2.20)). We relate these eigenfunctions to the patterns emerging at bifurcations of mixing. In particular, we show that a PF bifurcation results in a PLS with stationary coherent cluster, whereas an AH bifurcation leads to the creation of two moving clusters.

Following [11, 12], we employ the method used by Penrose in [35] to locate the roots of (3.1) in  $\mathbb{H}^+$ . To this end, let  $\mathcal{C}$  denote an oriented curve G(it),  $t \in \mathbb{R}$ . First, we establish certain qualitative properties of  $\mathcal{C}$ . To this end, we note that G is a holomorphic function on  $\mathbb{H}^+$  (cf. (2.16)). By the Paley-Wiener theorem, using (2.19), G can be extended analytically to the region Im z > -a. Further, we use the Sokhotski-Plemelj formula [38] to obtain

$$G(it + 0) = \pi g(t) + i \int_0^\infty \frac{g(t+s) - g(t-s)}{s} ds.$$
 (3.2)

This yields the following parametric equations for C:

Re 
$$z = \pi g(t)$$
,  
Im  $z = \int_0^\infty \frac{g(t+s) - g(t-s)}{s} ds$ , (3.3)

for  $t \in \mathbb{R}$ . It follows from (3.3) that  $\mathcal{C}$  lies in  $\overline{\mathbb{H}}^+$  and  $\mathcal{C}$  asymptotes onto the origin. Thus,  $\mathcal{C}$  is a bounded closed curve in  $\overline{\mathbb{H}}^+$  (see Fig. 1b).

#### 3.1 Unimodal g

We are now prepared to discuss the bifurcations in the KM. We start with the case of an even unimodal g (see Fig. 1a). Although the bifurcation of mixing leading to the transition



Chimeras Unfolded Page 7 of 19 46

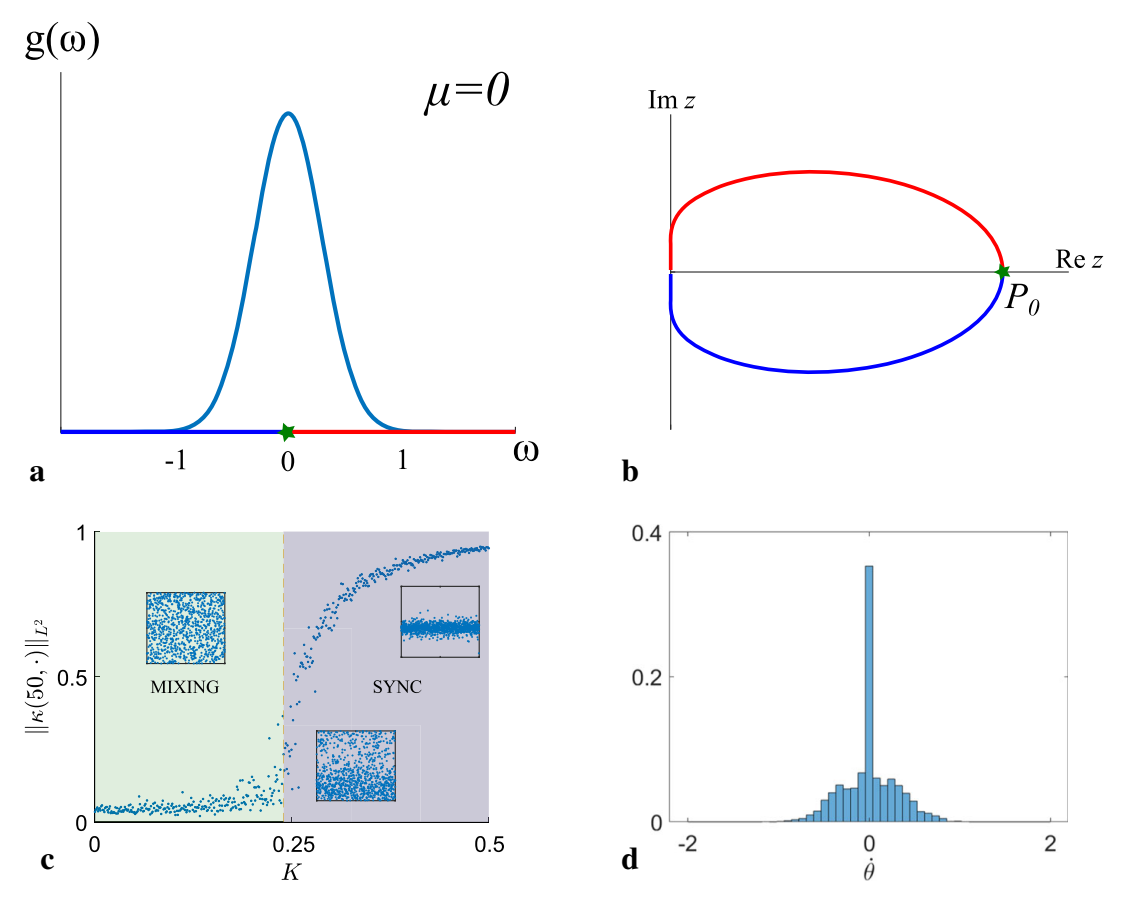


Fig. 1 a Graph of an even, unimodal probability density function g (Gaussian distribution with standard deviation  $\sigma=0.3$ ). **b** The corresponding critical curve  $\mathcal C$  intersects the positive real semiaxis at a unique point  $P_0$ . The preimage of  $P_0$  under G is indicated by the green star in **a**.  $P_0$  corresponds to the PF bifurcation of mixing resulting in a PLS at the critical value  $K_c=P_0^{-1}$  (see (3.1)), which is then gradually transformed into synchronous state (see (c)). c The bifurcation diagram for (1.1) with unimodal intrinsic frequency distribution and all-to-all coupling.  $\|\kappa(50,\cdot)\|_{L^2}$  is the the  $L^2$ -norm of the order parameter  $\kappa(T,\cdot)$  (cf. (2.4)) at time T=50, which is sufficient for transients to settle down. Each dot corresponds to the value of  $\|\kappa(50,\cdot)\|_{L^2}$  computed for a given value of K. Initial conditions and intrinsic frequencies were sampled from the uniform distribution on  $\mathbb{T}$  and Gaussian distribution with mean zero and standard deviation  $\sigma=0.3$ . Independent samples of the initial conditions and frequencies were used for each value of K. The insets contain snapshots  $\theta_i(50)$ ,  $i \in [100]$ , representative of patterns for three different regimes (from left to right): mixing, PLS, and synchronization. The regions of stability and instability of mixing separated by  $K=K_c$  are colored in green and blue respectively. **d** A histogram computed for a sample of velocities  $\dot{\theta}_i(50)$ ,  $i \in [100]$  for K=0.2505 just above the critical value  $K_c$ . The velocity distribution within the PLS near PF bifurcation is consistent with the qualitative features of the unstable mode (3.4)

to synchrony for such g is well understood (cf. [3, 11, 39, 40]), we use it as an example to explain the method using Penrose diagrams. Below, we will apply this method to study bifurcations in families of bi- and tri- modal distributions (Figs. 3, 7).

Using the symmetry of g, from (3.3) we see that  $\mathcal{C}$  is symmetric about the x-axis. It intersects the positive real semiaxis at a unique point  $P_0 = (x_0, 0), x_0 > 0$ . Further, note that  $G^{-1}(x_0) = 0$  (Fig. 3a, b). From the x-equation in (3.3) we find  $x_0 = \pi g(0)$ . By the Argument Principle, the number of roots of (3.1) in  $\mathbb{H}^+$  is equal to the winding number of  $\mathcal{C}$  about  $K^{-1}$  [35]. Since for  $K < K_c := (\pi g(0))^{-1}, K^{-1}$  lies outside  $\mathcal{C}$  (Fig. 1b), the winding number is 0. We conclude that for  $K < K_c$ , T has no eigenvalues with positive real parts. Thus, for  $K < K_c$ , mixing is linearly stable. In fact, it is asymptotically stable



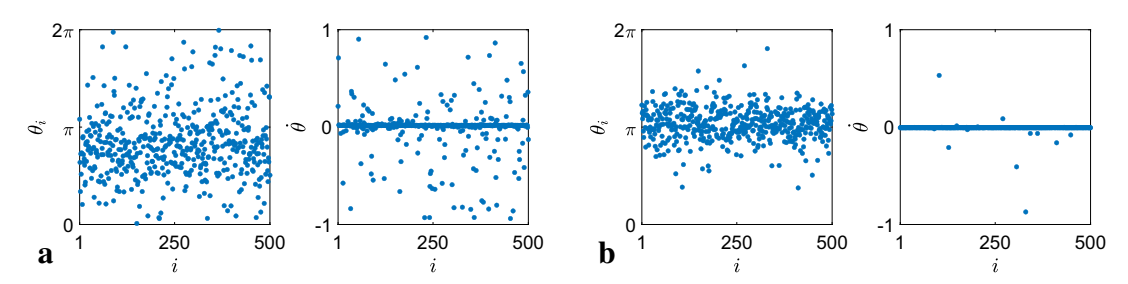


Fig. 2 The snapshots of oscillator positions  $\theta_i$  (50) and their velocities  $\dot{\theta}_i$  (50),  $i \in [100]$ , starting from uniform (on  $\mathbb{T}$ ) initial conditions. Oscillators are all-to-all coupled and the distribution of the intrinsic frequencies is the same as in Fig. 1. The snapshots in **a** were done for K = 0.275 just above the critical value  $K_c$ . The snapshots in **b** were done for K = 0.375. The number of drifting oscillators decreases for increasing values of K.

[7,Theorem 4.1]. For  $K > K_c$ , on the other hand, the winding number is 1. As  $K \to K_c + 0$ ,  $\lambda \to 0+$ , and at  $K = K_c$ , mixing undergoes a PF bifurcation [3]. Using (2.18) and (2.21), we compute the eigenfunction corresponding to  $\lambda = 0$ :

$$v_0(\omega, x) = \pi g(0)\delta_0(\omega) - i\mathcal{P}_0[g](\omega). \tag{3.4}$$

Each term on the right-hand side of (3.4) has a singularity at 0. The second term also has a regular component. This determines the structure of the PLS bifurcating from the mixing state (Fig. 1c). Since the coupling term in (1.1) is small near the onset of synchronization ( $\kappa \approx 0$ ), the unstable eigenfunction (3.4) effectively predicts the structure of the velocity distribution within the PLS. Specifically, the delta function on the right-hand side of (3.4) implies that the coherent cluster within the PLS is stationary. The regular component of  $i\mathcal{P}_0[g]$  yields the velocity distribution within the incoherent group. The combination of these two terms yields the velocity distribution within the PLS (Figs. 1d, 2a).

**Remark 3.1** It is known that the branch of solutions bifurcating from mixing at  $K_c$  supports PLS (cf. [25,§ 4]):

$$f_{PLS}(\theta, \omega) = \begin{cases} \frac{\sqrt{\omega^2 - (K\kappa)^2}}{|\omega - K\kappa \sin \theta|}, & |\omega| > K\kappa, \\ \delta_{\theta_{\omega}}, & |\omega| \le K\kappa, \end{cases}$$
(3.5)

where  $\theta_{\omega} \in [-\pi/2, \pi/2]$  is a root of

$$\sin\theta = \frac{\omega}{K\kappa}.$$

The continuous and singular components of  $f_{PLS}$  in (3.5) correspond to groups of drifting and phase locked oscillators respectively. Since  $\kappa$  remains bounded away from 0, for increasing values of K, the weight of the drifting oscillators diminishes and the resultant patterns become more and more coherent. In this paper, we call a solution synchronous rather than a PLS, when the mass of drifting oscillators becomes relatively small (Fig. 2). The empirical distinction between PLS and synchronous solutions can be formalized by introducing a bound on the weight of drifting oscillators:

$$\int_{\mathbb{T}\times\{|\omega|>K\kappa\}} f_{PLS}(\theta,\omega)d\theta d\omega < \epsilon,$$

for some fixed  $0 < \epsilon \ll 1$ . We do not introduce a quantitative threshold for coherent structures, because empirical identification of patterns suffices for the purposes of this work.



Chimeras Unfolded Page 9 of 19 46

## 3.2 Bimodal g

Next, we turn to the description of a bifurcation scenario connecting mixing to chimeras through 2–clusters. To this end, we continuously deform the unimodal distribution g into a bimodal distribution, preserving even symmetry as shown in Fig. 3a, b. In our numerical experiments, we use the following family of probability distribution functions:

$$g_{\sigma_1,\sigma_2}^{\mu}(x) = \frac{1}{2\sqrt{2\pi}} \left\{ \frac{e^{\frac{-(x+\mu)^2}{2\sigma_1^2}}}{\sigma_1} + \frac{e^{\frac{-(x-\mu)^2}{2\sigma_2^2}}}{\sigma_2} \right\}.$$
(3.6)

When  $\sigma_1 = \sigma_2 =: \sigma$ , we collapse indices into one  $g_{\sigma}^{\mu} := g_{\sigma,\sigma}^{\mu}$ . First, we keep  $\sigma_1 = \sigma_2 =: \sigma$  and increase  $\mu$  from zero. We want to understand how the critical curve changes as  $\mu$  is varied. The key events in the metamorphosis of  $\mathcal{C}$  are shown Fig. 3d, e.

For small  $\mu > 0$ ,  $C_{\mu}^{-1}$  is diffeomorphic to  $C_0$  in a neighborhood of  $P_0$ , the point of intersection of  $C_0$  with the real axis.

At a critical value  $\mu^* > 0$ ,  $C_{\mu^*}$  develops a cusp at  $P_{\mu^*}$  (see Fig. 3d). To identify the condition for the cusp, we look for the value of  $\mu$  at which the condition of the Inverse Function Theorem fails for G. By (3.3) this occurs when  $d\operatorname{Im} z(t)/dt|_{t=0} = 0$ , i.e.,

$$J[g_{\sigma}^{\mu^*}] := \int_0^{\infty} \frac{(g_{\sigma}^{\mu^*})'(s)}{s} ds = 0$$
 (3.7)

(see Fig. 4a).

For  $\mu > \mu^*$  there is a point on the real axis  $P_{\mu}$ , which has two preimages under G:  $\pm i \nu$  (Fig. 3b, e)<sup>2</sup>. Thus, for  $\mu > \mu^*$  mixing loses stability through the AH bifurcation and not through the PF bifurcation. At the AH bifurcation, T has a pair of complex conjugate eigenvalues  $\pm i \nu$ . The corresponding eigenfunctions are given by (2.18), (2.20)

$$v_{\pm i\nu + 0} = \pi g_{\sigma}^{\mu}(\pm \nu)\delta_{\pm \nu} - i\mathcal{P}_{\pm \nu}[g_{\sigma}^{\mu}]. \tag{3.8}$$

The first term on the right-hand side of  $v_{i\nu+0}$  (cf. (3.8)) is localized at  $\omega=\nu$ . The second term is singular at  $\nu$  too, but also has a regular component. The combination of of  $v_{i\nu+0}$  and  $v_{-i\nu+0}$  results in splitting the population into two groups of approximately equal size rotating with velocities centered around  $\pm\nu$ . We call this pattern a 2-cluster state. Thus, for  $\mu>\mu^*$  mixing bifurcates into a 2-cluster state. To estimate the group velocity for each cluster, we compute the arguments of the complex order parameters  $\Psi_n^{\pm}$  for each cluster:

$$|\kappa_n^{\pm}|e^{i\Psi_n^{\pm}} = \frac{1}{n^{\pm}} \sum_{j=1}^n e^{i\theta_j} \mathbf{1}_{\pm\omega_j > 0}, \quad n^{\pm} = \sum_{j=1}^n \mathbf{1}_{\pm\omega_j > 0}.$$
 (3.9)

The plots of  $\Psi_n^{\pm}$  in Fig. 5 confirm that the clusters move in the opposite directions at approximately constant speed.

At  $\mu = \mu^*$ , where the regions of the PF and AH bifurcations meet, we have a codimension–2 bifurcation, whose unfolding contains the transitions to synchronization, 2–clusters, and to chimeras, as we are going to see next. We now fix  $\mu > \mu^*$  and break the even symmetry of  $g_{\sigma}^{\mu}$  by decreasing  $\sigma_1$  and increasing  $\sigma_2$  (see Fig. 3c). This affects the critical curve  $\mathcal{C}_{\mu,\sigma_1,\sigma_2}$  in

<sup>&</sup>lt;sup>2</sup> The Penrose diagram similar to that in Fig. 3e was discussed in [11], but the connection to the AH bifurcation was not made.



<sup>&</sup>lt;sup>1</sup> From this point on, we explicitly indicate the dependence of C, x, and P on  $\mu$ .

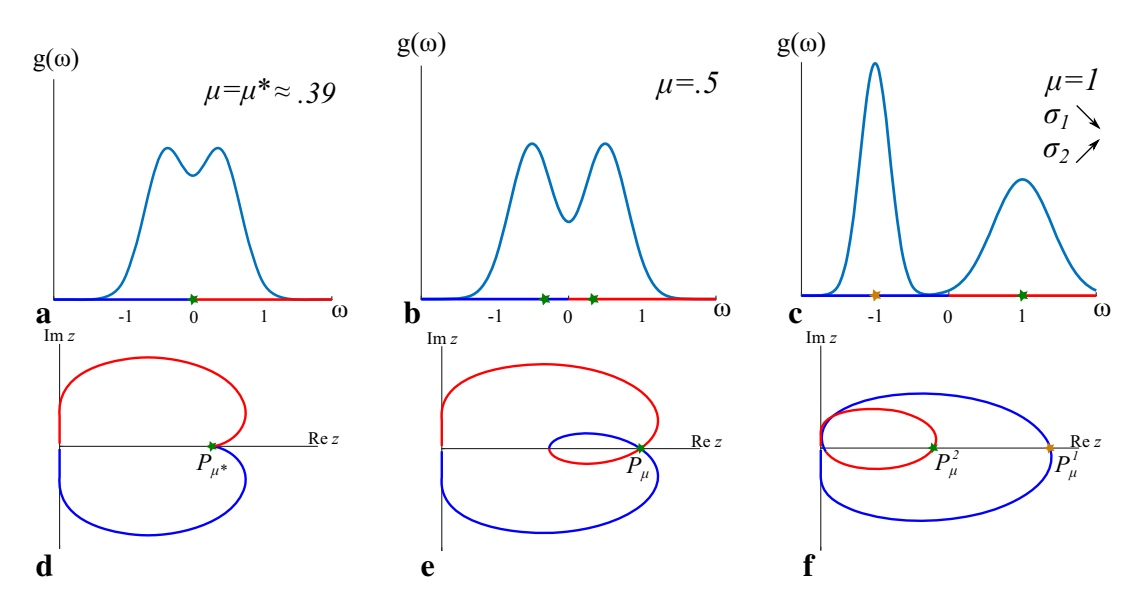


**Fig. 3** a-c Continuous deformation of the unimodal symmetric density g into a bimodal asymmetric one ( $\mathbf{c}$  and the plots of the corresponding critical curves ( $\mathbf{d}$  and  $\mathbf{f}$ ). At the critical value  $\mu = \mu^*$ ,  $\mathcal{C}_{\mu^*}$  develops a cusp ( $\mathbf{d}$ ). This corresponds to the codimension-2 bifurcation of mixing. The preimages of points of the intersection of the critical curve with the real axis  $P_{\mu}$  and  $P_{\mu}^{1,2}$  in  $\mathbf{d}$  and  $\mathbf{f}$  are indicated by stars in the corresponding plots in ( $\mathbf{a}$ - $\mathbf{c}$ )

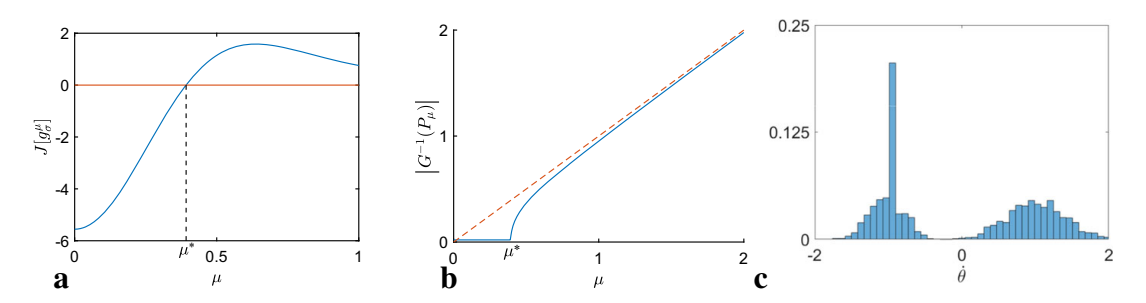
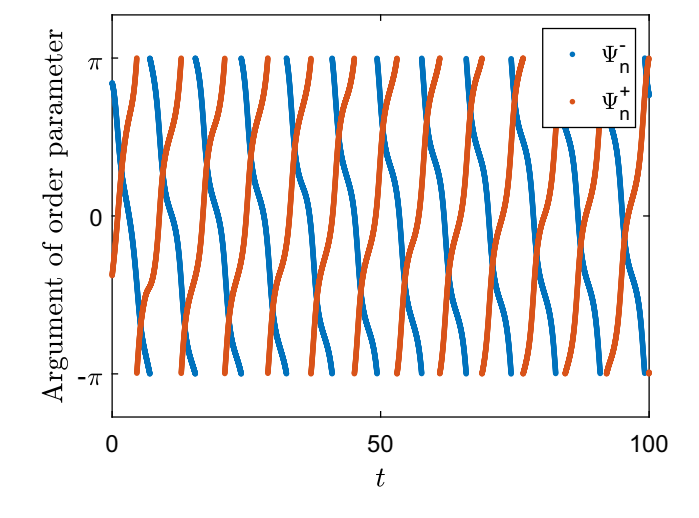


Fig. 4 a The plot of  $J[g_{\sigma}^{\mu}]$  vs  $\mu$  (cf. (3.7)). The zero of  $J[g_{\sigma}^{\mu}]$  determines the critical value  $\mu^*$ . b The plot of the absolute value of the two preimages  $G^{-1}(P_{\mu})$ . Note that for  $\mu > \mu^*$  outside a small neighborhood of  $\mu^*$ ,  $\left|G^{-1}(P_{\mu})\right| \approx \mu$ , i.e., the two preimages of  $P_{\mu}$  lie near the peaks of the density g. c The histogram of the velocity distribution within a chimera is consistent with the singular distribution  $v_{it_{\mu}+0}$  (cf. (3.10)). The parameter values used for plot  $\mathbf{c}$  are  $\mu=1$ ,  $\sigma_1=0.2$ ,  $\sigma_2=0.4$  and K=0.165.

Fig. 5 The plots of  $\Psi_n^+$  and  $\Psi_n^-$  (cf. (3.9)), the arguments of the order parameters computed for two groups with positive and negative intrinsic frequencies plotted for a 2-cluster state ( $\mu = 1$ ,  $\sigma_1 = \sigma_2 = 0.3$ , K = 0.375). As can be seen from this plot, the two clusters move with approximately constant speeds in the opposite directions





Chimeras Unfolded Page 11 of 19 46

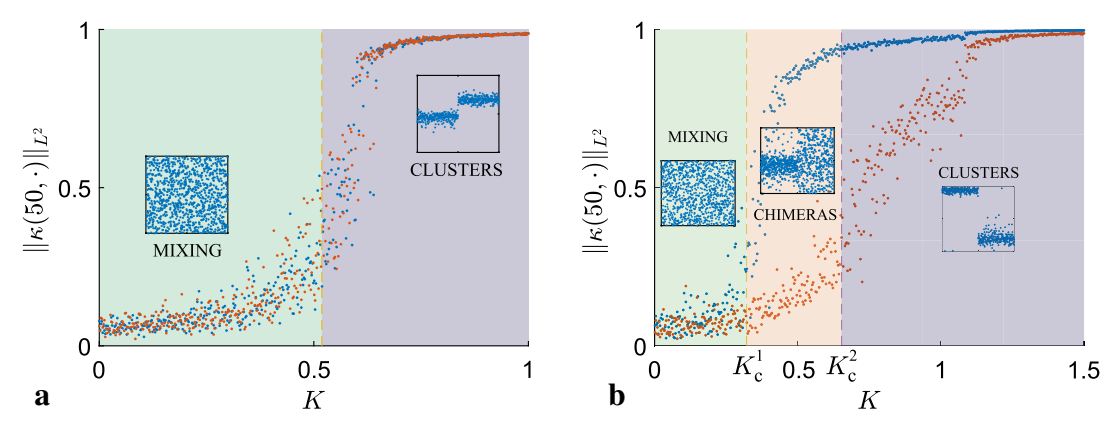


Fig. 6 The bifurcation diagrams corresponding to the symmetric and asymmetric bimodal distributions and all-to-all connectivity. The meaning of  $\|\kappa(50,\cdot)\|_{L^2}$  is the same as in the caption to Fig. 1. For simulations shown in **a**, we used probability density function  $g_{\sigma}^{\mu}$  with  $\mu = 1$  and  $\sigma = 0.3$  (cf. (3.6)). The graph of this function is shown in Fig. 3b. In b, we switched to  $g_{\sigma_1,\sigma_2}^{\mu}$  with  $\mu=1,\,\sigma_1=0.2,\,$  and  $\sigma_2=0.4.$  The initial conditions are the same as explained in the caption to Fig. 1. To highlight the distinction between the bifurcation scenarios for symmetric and asymmetric densities, we computed the order parameters separately for oscillators with negative and positive intrinsic frequencies. The value of  $\|\kappa(50,\cdot)\|_{L^2}$  is plotted in blue for the former group of oscillators and in red for the latter. In the symmetric case, the values of order parameters undergo transition from values close to 0 (mixing state) to 1 (synchronization) simultaneously. This results in the creation of a two-cluster state shown in the right inset in a. In the insets, the oscillators are split into two groups based on the sign of the corresponding intrinsic frequencies. The oscillators with negative frequencies appear on the left. The two clusters shown in the right inset in a rotate with near constant velocity in opposite directions. In the asymmetric case, the order parameter computed for the left cluster starts to increase around  $K_0^1$ , while the order parameter computed for the right cluster remains small. This results in the creation of the chimera state shown in the middle inset in b. The order parameter corresponding to the right cluster (plotted in red) starts to increase around  $K_c^2$ . From this point, the chimera state born at  $K_c^1$  is gradually transformed into a (moving) two-cluster state shown in the right inset in **b**. Eventually, the two-cluster state becomes stationary. The bifurcation that transforms a traveling two-cluster state into a stationary one is explained in [24, § 5.1] (see Fig. 11 in [24])

the following way. The point of double intersection  $P_{\mu}$  splits into two points of intersection with the real axis:  $P_{\mu}^{1}=(x_{\mu}^{1},0)$  and  $P_{\mu}^{2}=(x_{\mu}^{2},0)$  with  $0< x_{\mu}^{2}< x_{\mu}^{1}$  (see Fig. 3f). Note that the preimages of these points under G are still very close to the maxima of  $g_{\sigma_{1},\sigma_{2}}^{\mu}$  (see Fig. 3c and Fig. 4b). In particular, the preimage of  $P_{\mu}^{1}$  is approximately  $-i\,\mu$ , the center of the more localized peak of  $g_{\sigma_{1},\sigma_{2}}^{\mu}$ . This implies that mixing loses stability at  $K_{c}^{1}\approx(\pi\,g_{\sigma_{1},\sigma_{2}}^{\mu}(-\mu))^{-1}$ . The bifurcating eigenvalue  $\lambda=i\,\nu_{1}(\nu_{1}\approx-\mu)$  and the corresponding eigenfunction

$$v_{i\nu_1+0} = \pi g^{\mu}_{\sigma_1,\sigma_2}(\nu_1)\delta_{\nu_1} - i\mathcal{P}_{\nu_1}[g^{\mu}_{\sigma_1,\sigma_2}]. \tag{3.10}$$

Note that the first term on the right hand side of (3.10) is a singular distribution localized at  $\nu_1$ . The second term has a singularity at  $\nu_1$ , but its regular part has some weight near  $\nu_2 \approx \mu$ . These features translate into the velocity distribution within an emerging pattern: there is a tightly localized peak around  $-\mu$  (the coherent group) and a broader peak near  $\mu$  (the incoherent group) (Fig. 4c). The structure of the unstable eigenfunction suggests that just after the bifurcation the oscillators split into two groups. One group, formed by the oscillators with negative intrinsic frequencies, contains both phase locked and drifting oscillators, whereas the other group consists of drifting oscillators (see the snapshot in Fig. 6b). Such patterns with coexisting groups of drifting and coherent oscillators are called chimeras [1, 19, 28].

For increasing values of K, the chimera state is gradually transformed into a 2-cluster pattern (Fig. 4b). As in the situation described in Remark 3.1, there is no sharp boundary between the regions of chimeras and 2-clusters shown in Fig. 6b. Patterns of both types



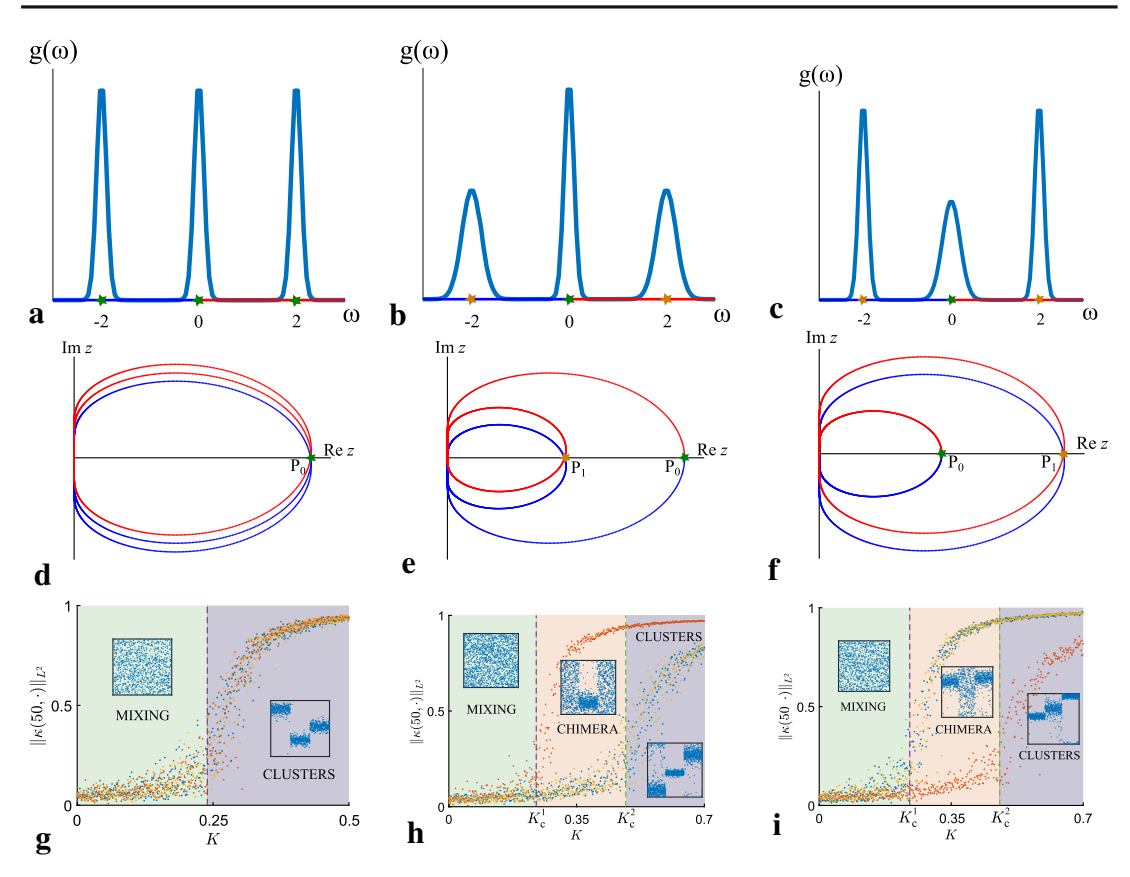
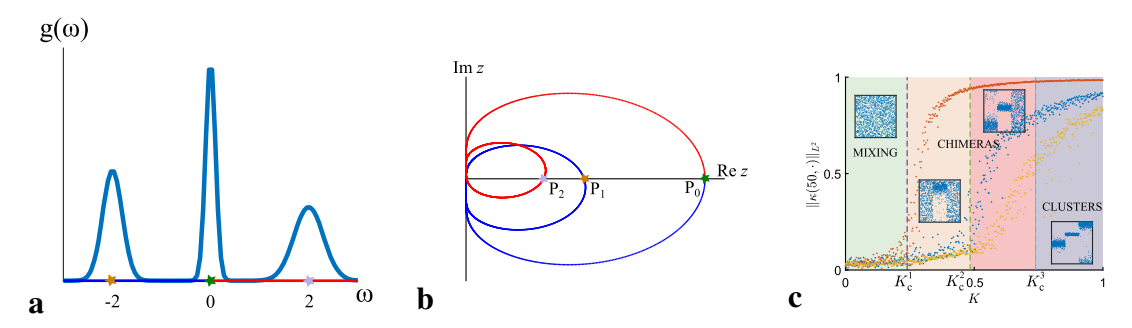


Fig. 7 a-c A family of trimodal probability distributions (3.11) with  $\mu=2$ : a)  $\sigma_1=\sigma_3=0.1976$ ,  $\sigma_2=0.2$ , b)  $\sigma_1=\sigma_3=0.2$ ,  $\sigma_2=0.1$ , c)  $\sigma_1=\sigma_3=0.1$ ,  $\sigma_2=0.1$ . d-f The corresponding critical curves. Under the deformation of the density functions, the point of triple intersection in d splits into a point of simple intersection and a point of double intersection e and f. Each point of simple intersection corresponds to a PF bifurcation producing a pattern with a stationary cluster, whereas a point of double intersection corresponds an AH bifurcation resulting in patterns with a pair of moving clusters. The bifurcation scenarios predicted by the diagrams in d-f with all-to-all coupling are shown in g-i. They are explained in the text. As in Fig. 6, oscillators are split into three groups by their intrinsic frequencies: (i)  $\omega < -\mu/2$ ; (ii)  $-\mu/2 \le \omega < \mu/2$ ; (iii)  $\omega \ge \mu/2$ 

contain phase locked and drifting oscillators. The difference between them lies in the degree of coherence within the two groups with positive and negative intrinsic frequencies. In the case of clusters, both groups are coherent, i.e., the weight of drifting oscillators is relatively small. In the case of chimeras, one group is incoherent. The difference in the coherence within the two groups of oscillators composing chimera states is clearly seen in the velocity histogram in Fig. 4c and in the plots of the order parameter computed separately for each group in Fig. 6b. The latter reveal that coherence builds up faster in the first 'coherent' cluster (the one that was more coherent from the start). The order parameter computed for the second cluster grows sharply near  $K_2^c$ , the second point of the intersection of the critical curve  $\mathcal{C}$  with the real axis  $P_{\mu}^2$  (see Fig. 3f). At  $K_2^c$  (already unstable) mixing undergoes the second bifurcation. While the secondary bifurcation of mixing is not formally connected to the transformations of the chimera state, the notable increase of coherence in the second cluster near  $K_c^2$  is an interesting artifact (Fig. 6b).



Chimeras Unfolded Page 13 of 19 46



**Fig. 8** Symmetry breaking in the trimodal distribution shown in Fig. 7b results in splitting of the point of the double intersection into two simple intersection points. Here  $\sigma_1 = 0.2$ ,  $\sigma_2 = 0.1$ ,  $\sigma_3 = 0.3$ . Thus, the Penrose diagram predicts a PF bifurcation and two secondary bifurcations. The former produces a chimera with the stationary coherent cluster in the middle ( $\mathbf{c}$ , beige). As in the bimodal case we observe a rapid increase of coherence in the two incoherent clusters near the first secondary bifurcation (see the border between the beige and the pink regions). Right after that point the numerical experiments show a chimera with two coherent clusters (a stationary cluster in the middle and a traveling one on the left) ( $\mathbf{c}$ , pink). For larger values of K we observe a three-cluster state with the stationary middle cluster and two clusters rotating in opposite directions ( $\mathbf{c}$ , purple)

## 3.3 Trimodal q

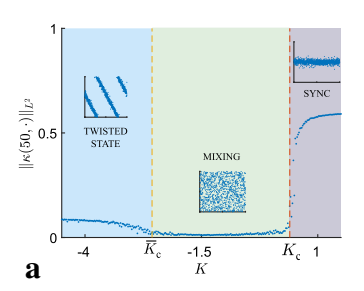
To give a more complete picture of possible bifurcation scenarios in the KM with multimodal distributions of the intrinsic frequencies, we discuss bifurcations in the KM with trimodal family of distributions. In the numerical experiments used in this section, we take the probability distribution functions of the following form:

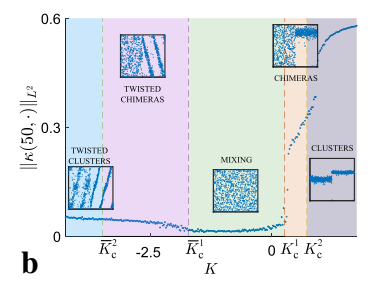
$$g_{\sigma_1,\sigma_2,\sigma_3}^{\mu}(x) = \frac{1}{3\sqrt{2\pi}} \left\{ \frac{e^{\frac{-(x+\mu)^2}{2\sigma_1^2}}}{\sigma_1} + \frac{e^{\frac{-x^2}{2\sigma_2^2}}}{\sigma_2} + \frac{e^{\frac{-(x-\mu)^2}{2\sigma_3^2}}}{\sigma_3} \right\}.$$
(3.11)

To study bifurcations in the model with trimodal frequency distribution we employ the same strategy as above. We first locate the highest codimension master bifurcation of mixing, whose unfolding contains all principal bifurcation scenarios. To this end, we fix  $\mu > 0$  and choose  $\sigma_1, \sigma_2, \sigma_3$  so that the critical curve  $\mathcal C$  has a point of triple intersection with the real axis  $P_0$  (see Fig. 7d). In our numerical simulations, we used  $\mu = 2$  and  $\sigma_2 = 0.2$ , and  $\sigma_1 = \sigma_3 \approx 0.1976$ , i.e., all peaks are practically the same (see Fig. 7a). The intersection point  $P_0$  has three preimages under G:  $G^{-1}(P_0) \approx \{\pm 2i, 0\}$ . Thus, the loss of stability of mixing takes place through a PF-AH bifurcation. The diagram in Fig. 7g shows the bifurcation of mixing producing a 3-cluster state. The middle cluster is stationary as implied by the PF bifurcation and the two outer clusters are moving with opposite velocities as implied by the AH bifurcation.

Next, we deform the distribution in Fig. 7a preserving even symmetry in two different ways. First, we increase  $\sigma_1$  and  $\sigma_3$  keeping them equal (see Fig. 7b). Under this deformation, the triple intersection point splits into a simple intersection point  $P_0$  and a point of double intersection  $P_1$  (see Fig. 7e). This results in a PF bifurcation followed by the AH bifurcation of mixing. The former produces a chimera state with a stationary middle cluster, which is further transformed into a three-cluster state with a stationary cluster in the middle and two rotating clusters on the sides (see Fig. 7h). An alternative scenario is shown in the last column of Fig. 7. This time the AH bifurcation comes first and, therefore, we get a chimera state with two traveling coherent clusters on the sides. For larger values of K, we arrive at







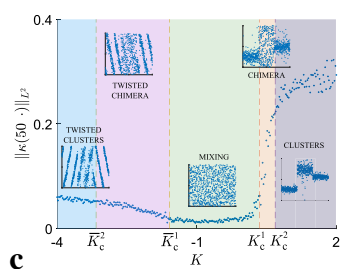


Fig. 9 Bifurcation diagrams for the KM with nonlocal nearest-neighbor coupling and uni-, bi-, and tri- modal frequency distributions shown in plots  $\bf a$ ,  $\bf b$ , and  $\bf c$  respectively. In all simulations the nearest neighbor coupling range is r=0.3. In ( $\bf a$ ) the unimodal distribution ( $\sigma=0.3$ ) results in a PF bifurcation leading to synchronization for positive K has a counterpart for K negative. The latter results in the emergence of stationary twisted states. The same principle applies to the bifurcation diagrams in  $\bf b$  and  $\bf c$ : bifurcations for positive K have mirror images for negative K with coherent structures superimposed on twisted states. For instance, diagram  $\bf b$  features twisted chimera and clusters of traveling twisted states generated from an asymmetric bimodal distribution with  $\mu=1$ ,  $\sigma_1=0.4$ ,  $\sigma_2=0.2$ . Using the trimodal distribution from Fig. 7 $\bf c$ , we obtain the 3-clusters shown in  $\bf c$ , two outer clusters contain traveling twisted states and the middle one presents a stationary twisted states. The cluster type (stationary vs traveling) is determined by the underlying bifurcation. The AH bifurcation results in a pair of traveling coherent structures, whereas the PF bifurcation produces a stationary one (see text for details). In the insets in  $\bf b$  and  $\bf c$ , the oscillators are grouped together by the values of intrinsic frequencies (see caption of Fig. 7 for details). The order in x is preserved within each group. The reordering is done to unveil patterns

the same three-cluster pattern as above (see Fig. 7i). Finally, we break the even symmetry of g by decreasing  $\sigma_2$  and increasing  $\sigma_3$ . Without symmetry constraints, the point of triple intersection splits into three simple points  $P_0$ ,  $P_1$ , and  $P_2$  (see Fig. 8b). The bifurcation diagram in Fig. 8c shows the chimera state born after the loss of stability of mixing followed by a series of transformations making clusters coherent one by one. The eventual state is a three-cluster state with one stationary cluster and two moving clusters (see Fig. 8c).

# **4 Adding Connectivity**

Network connectivity can have a profound effect on the spatial organization of chimera states [8]. In the previous section, we discussed bifurcation scenarios in the KM with all–to–all coupling, i.e., for  $W \equiv 1$ . In this case, the largest eigenvalue of W is 1 and the corresponding eigenfunction is  $w \equiv 1$ . There are no negative eigenvalues. This has the following implications. Mixing is stable for  $K \in (-\infty, K_c)$  and patterns emerging at the bifurcation at  $K_c$  are spatially homogeneous, because  $v_{\lambda}(\omega, x)$  in (2.18) does not depend on x. In general, W may have eigenvalues of both signs [6]. In this case, along with the bifurcations at positive  $K_c^1$  and  $K_c^2$  identified above there are negative counterparts at  $\bar{K}_c^2 < \bar{K}_c^1 < 0$ . The eigenfunctions corresponding to negative eigenvalues of W are no longer constant and they endow the bifurcating patterns (clusters and chimeras) with a nontrivial spatial organization. We refer an interested reader to [6, 8] for examples of the bifurcation scenarios in the KM with nonconstant W.

In the remainder of this section, we discuss how network organization may affect the spatiotemporal patterns in the context of the bifurcation scenarios identified in the previous sections. To this end, suppose W has eigenvalues of both signs and denote the largest positive and smallest negative eigenvalues of W by  $\mu^+$  and  $\mu^-$  respectively. Then the region of stability of mixing is bounded  $K \in (K_c^-, K_c^+)$ , with  $K_c^- < 0 < K_c^+$ . Furthermore, one of



Chimeras Unfolded Page 15 of 19 46

the eigenfunctions corresponding to  $\mu^-$  or  $\mu^+$  is not constant. Thus, the patterns emerging from one of the bifurcations will have spatial structure. To illustrate these effects, we consider the KM with nonlocal nearest neighbor coupling. To this end, let W(x, y) = V(x - y), where V was defined in (2.1). In this case,

$$W[f](x) = \int_0^1 V(x - y)f(y)dy.$$
 (4.1)

The eigenvalues of W can be computed explicitly

$$\mu_k = \int_0^1 V(x)e^{\pm 2\pi i kx} dx = \int_0^1 V(x)\cos(2\pi kx) dx, \quad k = 0, 1, 2, \dots$$

The corresponding eigenfunctions are  $w_k = e^{\pm 2\pi i k x}$ . The largest positive eigenvalue is  $\mu^+ = 2r$  (cf. [6,Lemma 5.3]). By  $k^* > 0$  denote the value of k corresponding to the smallest negative eigenvalue of W,  $\mu_{k^*}$ . The corresponding eigenfunctions are  $e^{2\pi i k^* x}$  and  $e^{-2\pi i k^* x}$ .

To explain the implications of the presence of the eigenvalues of both signs in the spectrum of W, we first turn to the unimodal distribution. If g is even and unimodal then the region of stability of mixing is a bounded interval  $(K_c^-, K_c^+)$  with  $K_c^- = \pi(g(0)\mu^-)^{-1}$  and  $K_c^+ = \pi(g(0)\mu^+)^{-1}$  [6]. At  $K_c^+$  we observe a familiar scenario of transition to synchronization (Fig. 9). At  $K_c^-$  the situation is different. The center subspace of the linearized problem in the Fourier space is spanned by

$$v_{\mu^{-}}^{(1)} = \Upsilon_0(\omega)e^{2\pi i k^* x}$$
 and  $v_{\mu^{-}}^{(2)} = \Upsilon_0(\omega)e^{-2\pi i k^* x}$ .

In the solution space, we therefore expect that

$$f(t, \theta, \omega, x) \sim \text{Re}\left(c_1 + c_2 \Upsilon_0(\omega) e^{2\pi i (\pm k^* x - \theta)}\right), \quad c_1, c_2 \in \mathbb{C}.$$

For the PLS emerging at the bifurcation, we see that the structure encoded in  $\Upsilon_0(\omega)$  is now superimposed onto a  $k^*$ -twisted state<sup>3</sup> (Fig. 9a). The same principle applies to all other bifurcation scenarios, which we discussed for bi- and trimodal distributions in the previous sections. Specifically, whenever a transition to coherence occurs whether in a cluster or in the entire population, the nascent coherent structure is superimposed onto a twisted state.

Plots b and c of Fig. 9 present bifurcation diagrams for families of bimodal and trimodal distributions. The bifurcations for positive K analyzed in the previous sections have counterparts for negative K. The latter feature (traveling) twisted states every time the transition to coherence takes place. The velocity of the twisted states is determined by the corresponding eigenfunctions of T as before. The appearance of twisted states in this model is a consequence of the form of coupling. Whenever W(x, y) = V(x - y) for some function V on a unit circle, the eigenfunctions of W are exponential functions  $e^{2\pi i kx}$ . By varying V, one can achieve a variety of spatial patterns born when mixing loses stability.

#### 5 Discussion

In conclusion, we recap the main results of this work and relate them to previous studies. In this paper, we studied bifurcations in the KM with multimodal frequency distributions. We showed that the loss of stability of mixing in this model leads to different patterns including stationary and traveling clusters and chimera states. In structured networks these patterns



<sup>&</sup>lt;sup>3</sup> Twisted states are also commonly referred to as splay states (cf. [41]).

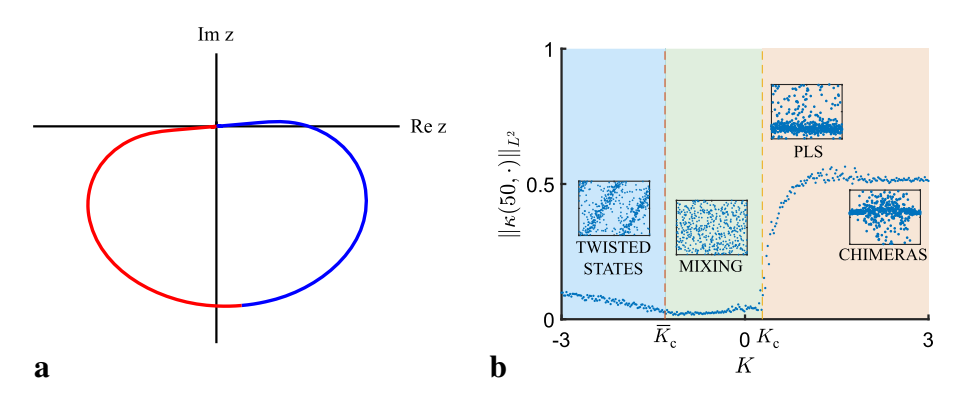


Fig. 10 a A nonzero phase lag  $\alpha=1.46$  in (1.1) results in a rotation of the critical curve in the complex plane. The critical curve intersects the positive semiaxis at a unique point, which determines the PF bifurcation. b The bifurcation diagram for the KM with  $\alpha=1.46$  and nearest neighbor coupling. Intrinsic frequencies are drawn from a unimodal Gaussian with  $\sigma=0.1$  and the nearest neighbor coupling range is r=0.35. The PF bifurcation at  $K_c>0$  results in a PLS. For larger values of K, the PLS is transformed into a chimera state that is similar to those observed in [31]. The PF bifurcation at  $K_c<0$  gives rise to twisted states

acquire additional spatial organization. In particular, bifurcations of mixing in the KM with nonlocal nearest-neighbor coupling give rise to twisted chimera states with regions of coherent behavior organized as stationary or traveling twisted states. The combination of the linear stability analysis, Penrose diagrams, and spectral properties of the graph limits provides information about the salient features of complex spatiotemporal patterns found in the KM after mixing loses stability. The type of the bifurcation determines the dynamical properties of the nascent patterns: the PF bifurcation results in one or more stationary clusters, whereas the AH bifurcation produces traveling clusters. Furthermore, we described a codimension-2 and a codimension-3 bifurcations of mixing, whose unfoldings contain transitions to stationary and traveling clusters and chimera states in the KM with bi- and trimodal frequency distributions respectively (Figs. 6, 7, 8). To locate the bifurcations of mixing leading to clusters or chimera states we used Penrose diagrams, which reduce the problem to the analysis of geometric and topological properties of a closed critical curve. Once the bifurcations are found, the emerging patterns are determined from the analysis of the unstable modes, i.e., the eigenfunctions of the linearized operator corresponding to the eigenvalues with zero real parts. In particular, the structure of the bifurcating eigenfunctions (viewed as tempered distributions) translates into the structure of the velocity distributions of emerging coherent structures.

There have been several previous studies of the KM with bimodal distribution. A review of the previous work in this direction can be found in [23]. In particular, as mentioned in [23], Kuramoto proposed a scenario for the onset of synchronization in the model with symmetric bimodal frequency distribution (cf. [18]). Specifically, he conjectured that in the bimodal case the onset would take place that  $K_c \approx (\pi g_{\sigma}^{\mu}(\mu))^{-1}$  and would lead to formation of a pair of clusters rotating in opposite directions. A detailed bifurcation diagram for the KM with symmetric bimodal Lorentz distribution was obtained in [23]. The analysis of bifurcations in this work exploited the Ott-Antonsen reduction [33]. In [23], one can also find information about global bifurcations in this system. Our results are local, but they do not rely on the Ott-Antonsen reduction and apply to a wide class of frequency distributions. Both the results in [23] and in the present study confirm Kuramoto's conjecture about the onset of synchronization in the bimodal case, provided the peaks of the bimodal distribution are well separated. Indeed, as shown in Subsection 3.2 when peaks in the bimodal distribution are not well separated, the system undergoes a PF bifurcation leading to PLS rather than cluster



Chimeras Unfolded Page 17 of 19 46

formation, in agreement with findings in [23]. Traveling chimera states similar to twisted states shown in Fig. 9b were identified in the KM with identical frequencies in [41]. In [41] the coherent structure is local in both x and  $\theta$ , resulting in just a small coherent portion of a twisted state that travels in the x-direction, whereas in our setting, coherent twisted states (extending over the entire ranges of x and  $\theta$ ) coexist with incoherent oscillators. The fragmentation of patterns into (coherent and incoherent) clusters in the KM model discussed in [41] was due to the multimodal structure of the kernel V (cf. (4.1)) rather than the structure of the frequency distribution as in the present study (see also [32] for analysis of related patterns). It would be interesting to apply the method of the present paper to study patterns in the KM with multimodal coupling functions like those considered in [41]. The asymmetry in the nonlocal coupling can make coherent structures travel along the ring (cf. [29]). This is different from the mechanism for rotating clusters and chimera states identified in Section 3.2, where the AH bifurcation not the asymmetry is responsible for rotation.

The first examples of chimera states were studied in the KM with identical frequencies [1, 19]. Since then chimera states were obtained in many different settings (see, e.g., [13, 20, 26, 34, 37]). In this work, we described chimera states in the KM with random frequencies sampled from multimodal distributions. To relate chimera states in the KMs with constant and random frequencies, consider the setting used in [27, 31]: identical frequencies, nearestneighbor coupling, and phase lag  $\alpha$  such that  $0 < \pi/2 - \alpha \ll 1$ . To match this setting using the KM with random frequencies, we take the Gaussian distribution centered at 0 with a small standard deviation  $\sigma = 0.1$ . All other parameters are the same as in [31]. It turns out that even a very localized probability distribution for  $\omega_i$ 's leads to important changes in the phase space when compared to the constant frequency setting. For the system with random albeit localized frequencies, the critical curve is shown in Fig. 10a. As before, there is a single point of intersection with the positive semiaxis. It corresponds to a PF bifurcation of mixing, giving rise to a PLS (Fig. 10b). For larger K, the PLS is transformed into a chimera state, which looks just like in the model with identical frequencies. Despite visual similarity, there is an important distinction between chimeras obtained in these two settings. In the model with identical frequencies, one has to carefully choose initial conditions mimicking the structure of a chimera state, otherwise, the trajectories converge to the synchronous state [1, 19]. It turns out that with random frequencies even for very small  $\sigma$ , no fine tuning of initial conditions is needed. Chimera states become very robust with respect to initial conditions. In particular, chimera states shown in the inset of Fig. 10b were obtained using initial conditions taken from the uniform distribution on  $\mathbb{T}$ .

Since their discovery chimeras have appealed to a broad community of mathematicians and physicists as a stark example of highly heterogeneous structures produced by homogeneous systems. It is important to note that even for the KM with identical frequencies as in [1, 19, 27], the setting is not completely homogeneous. A heterogeneous initial condition is still needed to generate chimera states. To compare this with the random frequencies setting, let us rewrite (1.1) as

$$\dot{\theta}_i = \omega_i + \frac{2K}{n} \sum_{j=1}^n a_{ij}^n \sin(\theta_j - \theta_i + \alpha),$$

$$\dot{\omega}_i = 0, \quad i \in [n].$$
(5.1)

Note that the right-hand sides in all equations have the same form, i.e., the system is homogeneous. The heterogeneity enters only through the initial condition. In this respect, our setting is not different from that in [1, 19, 27].



The coexistence of coherence and incoherence is arguably the most interesting effect in the theory of synchronization and possibly in nonlinear science in general discovered in the past two decades. Despite intense research chimera states still present many challenging questions to the nonlinear science community. There is no consensus on how to define chimera states. Further, the theory is only available for chimeras lying in the Ott-Antonsen manifold, which is an elegant but a very special case. In this work, we suggest a new way for studying chimera states based on the combination of the linear stability analysis of mixing and a beautiful method of Penrose for the Vlasov equation in plasma physics. This approach yields a new qualitative description of chimera states. Our results are universal in the sense that the structure and bifurcations of spatiotemporal patterns are explained in terms of the qualitative properties of the distribution of intrinsic frequencies and network topology, and, thus, are relevant for interacting particle systems of all scales from neuronal networks to power grids to astrophysics.

**Acknowledgements** The authors thank Oleh Omelchenko for illuminating discussions on chimera states. This work was supported in part by NSF grant DMS 2009233 (to GSM). Numerical simulations were completed using the high performance computing cluster (ELSA) at the School of Science, The College of New Jersey. Funding of ELSA is provided in part by NSF OAC-1828163. MSM was additionally supported by a Support of Scholarly Activities Grant at The College of New Jersey.

**Data Availability** Data sharing is not applicable to this article as no datasets were generated or analysed during the current study.

## References

- 1. Abrams, D.M., Strogatz, S.H.: Chimera states in a ring of nonlocally coupled oscillators. Int. J. Bifur. Chaos Appl. Sci. Eng. **16**(1), 21–37 (2006)
- 2. Abrams, D.M., Mirollo, R., Strogatz, S.H., Wiley, D.A.: Solvable model for chimera states of coupled oscillators. Phys. Rev. Lett. **101**, 084103 (2008)
- 3. Chiba, H.: A proof of the Kuramoto conjecture for a bifurcation structure of the infinite-dimensional Kuramoto model. Ergodic Theory Dynam. Syst. **35**(3), 762–834 (2015)
- 4. Chiba, H.: A spectral theory of linear operators on rigged Hilbert spaces under analyticity conditions. Adv. Math. **273**, 324–379 (2015)
- 5. Chiba, H.: A Hopf bifurcation in the Kuramoto-Daido model (2016). arXiv:1610.02834
- 6. Chiba, H., Medvedev, G.S.: The mean field analysis of the Kuramoto model on graphs I. The mean field equation and transition point formulas. Discret. Contin. Dyn. Syst. **39**(1), 131–155 (2019)
- 7. Chiba, H., Medvedev, G.S.: The mean field analysis of the Kuramoto model on graphs II. Asymptotic stability of the incoherent state, center manifold reduction, and bifurcations. Discret. Contin. Dyn. Syst. **39**(7), 3897–3921 (2019)
- 8. Chiba, H., Medvedev, G.S., Mizuhara, M.S.: Bifurcations in the Kuramoto model on graphs. Chaos 28(7), 073109, 10 (2018)
- 9. Chiba, H., Medvedev, G.S., Mizuhara, M.S.: Instability of mixing in the Kuramoto model: from bifurcations to patterns (2020). arXiv:2009.00103
- 10. Chiba, H., Medvedev, G.S., Mizuhara, M.S.: Bifurcations and patterns in the Kuramoto model with inertia (2021)
- 11. Dietert, H.: Stability and bifurcation for the Kuramoto model. J. Math. Pures Appl. (9) **105**(4), 451–489 (2016)
- 12. Dietert, H., Fernandez, B.: The mathematics of asymptotic stability in the Kuramoto model. Proceedings A 474(2220), 20180467, 20 (2018)
- 13. Dudkowski, D., Maistrenko, Y., Kapitaniak, T.: Occurrence and stability of chimera states in coupled externally excited oscillators. Chaos **26**(11), 116306, 9 (2016)
- 14. Eidelman, Y., Milman, V., Tsolomitis, A.: Functional Analysis, Graduate Studies in Mathematics, vol. 66. American Mathematical Society, Providence, RI (2004)
- 15. Georgi, S.: Medvedev, The continuum limit of the Kuramoto model on sparse random graphs. Commun. Math. Sci. 17(4), 883–898 (2019)



Chimeras Unfolded Page 19 of 19 46

16. John David Crawford: Amplitude expansions for instabilities in populations of globally-coupled oscillators. J. Stat. Phys. **74**(5–6), 1047–1084 (1994)

- 17. Kaliuzhnyi-Verbovetskyi, D., Medvedev, G.S.: The mean field equation for the Kuramoto model on graph sequences with non-Lipschitz limit. SIAM J. Math. Anal. **50**(3), 2441–2465 (2018)
- Kuramoto, Y.: Chemical Oscillations, Waves, and Turbulence. Springer Series in Synergetics, vol. 19. Springer, Berlin (1984)
- 19. Kuramoto, Y., Battogtokh, D.: Coexistence of coherence and incoherence in nonlocally coupled phase oscillators. Nonlinear Phenomena Complex Syst. **5**, 380–385 (2002)
- Laing, R.C.: The dynamics of chimera states in heterogeneous Kuramoto networks. Physics D 238(16), 1569–1588 (2009)
- Lancellotti, C.: On the Vlasov limit for systems of nonlinearly coupled oscillators without noise. Transport Theory Stat. Phys. 34(7), 523–535 (2005)
- 22. Lovász, L.: Large Networks and Graph Limits. AMS, Providence, RI (2012)
- 23. Martens, E.A., Barreto, E., Strogatz, S.H., Ott, E., So, P., Antonsen, T.M.: Exact results for the Kuramoto model with a bimodal frequency distribution. Phys. Rev. E (3) **79**(2), 026204, 11 (2009)
- 24. Medvedev, G.S., Mizuhara, M.S.: Stability of clusters in the second-order Kuramoto model on random graphs. J. Stat. Phys. **182**(2), 30 (2021)
- 25. Mirollo, R., Strogatz, S.H.: The spectrum of the partially locked state for the Kuramoto model. J. Nonlinear Sci. 17(4), 309–347 (2007)
- 26. Nkomo, S., Tinsley, M.R., Showalter, K.: Chimera and chimera-like states in populations of nonlocally coupled homogeneous and heterogeneous chemical oscillators. Chaos **26**(9), 094826, 10 (2016)
- 27. Omel'chenko, O.E.: Coherence-incoherence patterns in a ring of non-locally coupled phase oscillators. Nonlinearity **26**(9), 2469 (2013)
- 28. Omel'chenko, O.E.: The mathematics behind chimera states. Nonlinearity 31(5), R121–R164 (2018)
- 29. Omel'chenko, O.E.: Traveling chimera states. J. Phys. A **52**(10), 104001 (2019)
- 30. Omel'chenko, O.E., Maistrenko, Y.L., Tass, P.A.: Chimera states: the natural link between coherence and incoherence. Phys. Rev. Lett. **100**, 044105 (2008)
- 31. Omel'chenko, O.E., Wolfrum, M., Maistrenko, Y.L.: Chimera states as chaotic spatiotemporal patterns. Phys. Rev. E **81**(6), 065201 (2010)
- 32. Omel'chenko, O.E., Wolfrum, M., Laing, C.R.: Partially coherent twisted states in arrays of coupled phase oscillators. Chaos **24**(2), 023102 (2014)
- 33. Ott, E., Antonsen, T.M.: Low dimensional behavior of large systems of globally coupled oscillators. Chaos **18**(3), 037113, 6 (2008)
- Panaggio, J.M., Abrams, D.M.: Chimera states: coexistence of coherence and incoherence in networks of coupled oscillators. Nonlinearity 28(3), R67–R87 (2015)
- 35. Penrose, O.: Electrostatic instabilities of a uniform non-Maxwellian plasma. Phys. Fluids **3**(2), 258–265 (1960)
- 36. Rodrigues, F.A., Peron, T.K.D.M., Ji, P., Kurths, J.: The Kuramoto model in complex networks. Phys. Rep. **610**, 1–98 (2016)
- 37. Schmidt, L., Schönleber, K., Krischer, K., García-Morales, V.: Coexistence of synchrony and incoherence in oscillatory media under nonlinear global coupling. Chaos **24**(1), 013102, 7 (2014)
- 38. Simon, B.: Basic Complex Analysis, A Comprehensive Course in Analysis, Part 2A. American Mathematical Society, Providence, RI (2015)
- 39. Strogatz, H.S.: From Kuramoto to Crawford: exploring the onset of synchronization in populations of coupled oscillators. Physics D **143**(1–4), 1–20 (2000)
- 40. Strogatz, S.H., Mirollo, R.E.: Stability of incoherence in a population of coupled oscillators. J. Stat. Phys. **63**(3–4), 613–635 (1991)
- 41. Xie, J., Knobloch, E., Kao, H.-C.: Multicluster and traveling chimera states in nonlocal phase-coupled oscillators. Phys. Rev. E **90**, 022919 (2014)

**Publisher's Note** Springer Nature remains neutral with regard to jurisdictional claims in published maps and institutional affiliations.

